

AD-A067 272

VIRGINIA POLYTECHNIC INST AND STATE UNIV BLACKSBURG --ETC F/G 8/2
ORBITAL PHOTOGRAMMETRIC TRIANGULATION WITH DYNAMICAL CONSTRAINT--ETC(U)
MAR 79 J L JUNKINS, M RAJAN, J D TURNER

DAAG29-77-6-0018

ARO-13794.2-65

NL

UNCLASSIFIED

| OF |

AD
A067 272



END
DATE
FILMED

6 --79

DDC

DA067272

DDC FILE COPY

18

ARO

19

13794.2-GS and

12

ARO

15551.1-GS

6 ORBITAL PHOTOGRAMMETRIC TRIANGULATION
WITH DYNAMICAL CONSTRAINTS.

9

FINAL REPORT.

LEVEL II

10

Prepared by:

John L./Junkins,
Mahesh/Rajan
James D./Turner

11

Mar 1979

12 54p

U. S. Army Research Office

DDC
RECEIVED
APR 10 1979
C

15

Contracts Numbers: ✓ DAAG29-77-G-0018,
✓ DAAG29-78-G-0043

Engineering Science and Mechanics Department
Virginia Polytechnic Institute and State University
Blacksburg, Virginia 24061

APPROVED FOR PUBLIC RELEASE;
DISTRIBUTION UNLIMITED.

79 04 09 01 404 722

mt

14
20-1-1951
AR 13-104-2-1-104
10-1-1951

THE FINDINGS IN THIS REPORT ARE NOT TO BE
CONSTRUED AS AN OFFICIAL DEPARTMENT OF
THE ARMY POSITION, UNLESS SO DESIGNATED
BY OTHER AUTHORIZED DOCUMENTS.

TABLE OF CONTENTS

	<u>Page</u>
FOREWARD	11
1.0 INTRODUCTION	1
2.0 DYNAMICALLY CONSTRAINED PHOTOGRAMMETRIC TRIANGULATION: SUMMARY OF BASIC EQUATIONS	2
3.0 BATCH TRIANGULATION EXAMPLES	26
4.0 SEQUENTIAL TRIANGULATION EXAMPLE	34
5.0 CONCLUSIONS AND RECOMMENDATIONS	35
6.0 REFERENCES	36
APPENDIX A COORDINATE FRAME NOMENCLATURE AND KINEMATICAL RELATIONSHIPS	37
REPORT DOCUMENTATION DATA	50

ACCESSION for	
NTIS	White Section <input checked="" type="checkbox"/>
BDC	Buff Section <input type="checkbox"/>
UNANNOUNCED	<input type="checkbox"/>
JUSTIFICATION	<input type="checkbox"/>
BY	
DISTRIBUTION	
IDENTITY CODES	
SPECIAL	
A	

1 79 04 09 01

FORWARD

This document represents the final report under Contract DAAG29-78-G-0043, issued by

U. S. Army Research Office
P. O. Box 12211
Research Triangle Park, NC 27709

The authors appreciate the guidance of Dr. Steven Mock, Director of the Geosciences Division at USARO. The capable technical liasion of the following individuals:

Dr. Amando Mancini
Defense Mapping Agency Headquarters
Washington, D. C.
(Formerly, Director of the Research Institute at the U. S.
Army Engineer Topographic Labortories, Ft. Belvoir, VA)

Mr. L. A. Gambino, Director
Computer Science Laboratories
U. S. Army Engineer Topographic Laboratories
Ft. Belvior, VA

is greatly appreciated.

1.0 INTRODUCTION

We address here methods for triangulating orbital frame photography with rigorous accounting for spacecraft dynamics. Triangulation of *orbital* photography was established as an important survey tool, by the extensive mapping of the Moon accomplished by triangulation of orbital photography (beginning with the Lunar orbiter photography and continuing through the Appolo missions), and by more recent extra-terrestrial and terrestrial applications and studies.

Several issues need to be focused to appreciate the developments herein. Dynamical models of the camera bearing vehicle's motion, from one view, are unnecessary. As has been the tradition in triangulation of aerial photography (and mostly, orbital photography), it is possible to construct workable triangulation algorithms based solely upon principles of geometric optics. Perhaps the first question a skeptic might raise is: "Why clutter the (otherwise algebraic equation) scene with differential equations that must be solved numerically?" Enforcement of dynamical constraints imposes a physical truth (to an essentially negligible degree of approximation, the camera motion *is* governed exactly by Newton's laws of motion) - as a direct consequence of introducing dynamical constraints, one would expect to more closely recover the true camera position. The number of unknown parameters subject to differential correction is usually reduced as a consequence of introducing dynamical constraints; thus the normal equations have correspondingly reduced dimensions. Thus computer storage, run time, and precision considerations generally favor the dynamically constrained approach. The use of a dynamical model in orbital triangulation allows

one to restructure the triangulation process as an "iterative, extended Kalman estimation algorithm" with most significant computational advantages.

The above comments are fully supported by the results presented herein.

2.0 DYNAMICALLY CONSTRAINED TRIANGULATION: SUMMARY OF BASIC EQUATIONS

2.1 Colinearity Equations

In the process of satellite photogrammetric triangulation, the earth fixed object space coordinates of various earth surface features can be deduced from satellite photograph coordinates of the images of those features. The fundamental mathematical transformation central to this process is based solely on the principles of geometric optics and can be deduced from the geometry shown in Figures 1 and 2. This transformation (the colinearity equations) can be written [1] as

$$x_p = x_o - f \left[\frac{C_{11}(X_p - X_c) + C_{12}(Y_p - Y_c) + C_{13}(Z_p - Z_c)}{C_{31}(X_p - X_c) + C_{32}(Y_p - Y_c) + C_{33}(Z_p - Z_c)} \right] \quad (1a)$$

$$y_p = y_o - f \left[\frac{C_{21}(X_p - X_c) + C_{22}(Y_p - Y_c) + C_{23}(Z_p - Z_c)}{C_{31}(X_p - X_c) + C_{32}(Y_p - Y_c) + C_{33}(Z_p - Z_c)} \right] \quad (1b)$$

Equations (1) project the position of a point located at *object* coordinates (X_p, Y_p, Z_p) into its *image* plane coordinates (x_p, y_p) for a camera with principal point offset (x_o, y_o) and focal length f . The perspective center of the camera is located at *object* space coordinates (X_c, Y_c, Z_c) . The *image* space (x,y,z) axes are oriented relative to the *object* space (X,Y,Z) axes by the direction cosines $C_{\ell m}$; $\ell, m = 1, 2, 3$. Equations (1) can be written functionally as

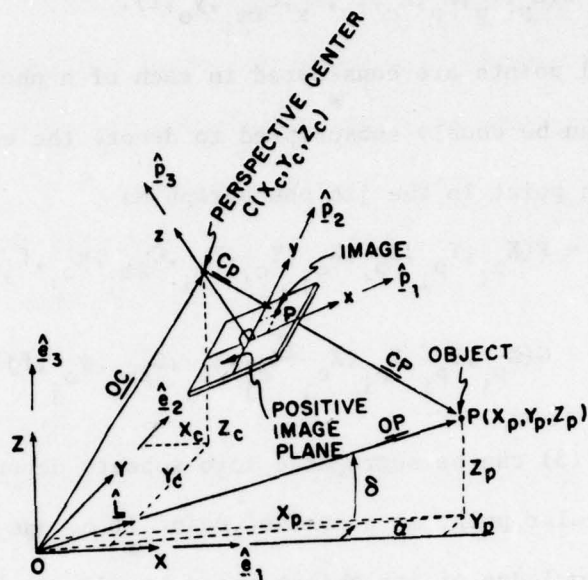


Figure 1 Co-Linearity of Perspective Center, Image, and Object

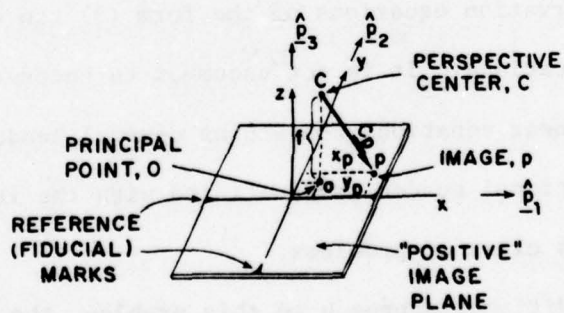


Figure 2 Photographic Coordinate System

$$\begin{aligned}x_p &= F(X_p, Y_p, Z_p, X_c, Y_c, Z_c, C_{lm_j}, x_o, f) \\y_p &= G(X_p, Y_p, Z_p, X_c, Y_c, Z_c, C_{lm_j}, y_o, f).\end{aligned}\tag{2}$$

If several points are considered in each of n photographs, Equations (1) and (2) can be doubly subscripted to denote the equations corresponding to the i th point in the j th photograph as

$$\begin{aligned}x_{p_{ij}} &= F(X_{p_i}, Y_{p_i}, Z_{p_i}, X_{c_j}, Y_{c_j}, Z_{c_j}, C_{lm_j}, x_{o_j}, f_j) \\y_{p_{ij}} &= G(X_{p_i}, Y_{p_i}, Z_{p_i}, X_{c_j}, Y_{c_j}, Z_{c_j}, C_{lm_j}, y_{o_j}, f_j).\end{aligned}\tag{3}$$

Equations (3) can be segregated into subsets depending on whether or not the particular point is a *control point* (i.e. one for which there exists apriori knowledge of its object space coordinates). Other points having distinctly measurable image plane coordinates in two or more photographs are unknown and are called *pass points*. Depending upon the number of photographs in a strip, the number of strips with sidelap, the number and distribution of control points, the number of pass points and the manner in which they are shared by adjacent photographs, an intimidating variety of observation equations of the form (3) can be defined in practical applications. It is not uncommon to encounter several thousand such nonlinear equations containing several hundred unknowns. An obvious computational burden is associated with the least squares solution of this class of problems.

In the traditional approach to this problem, the camera center coordinates $(X_{c_j}, Y_{c_j}, Z_{c_j})$ and three camera orientation angles $(\phi_j, \theta_j, \psi_j)$ for each photograph (it is possible to replace the direction cosines C_{lm} ; as functions of three orientation angles), as well as the pass point coordinates have been treated as independent unknowns. The introduction of orbital dynamical constraints, conceived by Brown [2,3]

the elimination of the $3n$ (n = number of photographs) camera center coordinates in favor of 6 osculating orbital elements. One purpose of this work is to carry the incorporation of dynamical constraints to its logical conclusion through rigorous satisfaction of the satellite equations of rotational motion. This process allows the further reduction of unknowns from $3n$ orientation angles to 6 osculating attitude elements or constants of the rotational motion.

2.2 Orbital Dynamical Constraints

The essence of orbit constrained photogrammetry is the recognition that the camera exposure stations along a given strip of n photographs are dynamically constrained according to

$$\begin{aligned} X_{c_j} &= X_c(t_j, c_1, c_2, \dots, c_6) \\ Y_{c_j} &= Y_c(t_j, c_1, c_2, \dots, c_6) \quad j = 1, 2, \dots, n, \\ Z_{c_j} &= Z_c(t_j, c_1, c_2, \dots, c_6) \end{aligned} \quad (4)$$

where Equations (4) are functional representations of the solution of the spacecraft's translational equations of motion. The 6 constants (c_1, \dots, c_6) can be any set of initial conditions or osculating orbital elements which uniquely define the orbit. The least squares solution of the photogrammetry problem is modified to include the dynamical constraints as follows: Current estimates of c_1, c_2, \dots, c_6 are used in Equations (4) to compute $X_{c_j}, Y_{c_j}, Z_{c_j}$ at each photograph exposure time t_j , the resulting estimates of camera exposure coordinates are used in Equations (3) together with the other parameter estimates ($X_{p_1}, Y_{p_1}, Z_{p_1}, \phi_j, \theta_j, \psi_j, x_{o_j}, y_{o_j}, f_j$) to determine current computed values of $x_{p_{ij}}, y_{p_{ij}}$ which are in turn differenced from the corresponding observed values to find the current residual vector. The partial derivatives of the

observation Equations (3) with respect to the orbital elements, c_1, c_2, \dots, c_6 (the elements of the "A" matrix) are determined by the chain differentiation rule applied to Equations (3) and (4). For example

$$\frac{\partial x_{p_{ij}}}{\partial c_1} = \frac{\partial F}{\partial x_{c_j}} \frac{\partial x_{c_j}}{\partial c_1} + \frac{\partial F}{\partial y_{c_j}} \frac{\partial y_{c_j}}{\partial c_1} + \frac{\partial F}{\partial z_{c_j}} \frac{\partial z_{c_j}}{\partial c_1}.$$

The partial derivatives with respect to the other parameters are identical in form to the corresponding equations for unconstrained photogrammetry. Depending on problem requirements, various specific forms of Equations (4) are available and the corresponding partial derivatives readily obtainable. Further discussion of orbital constraints is found in the work of Brown [2,3], Light [4], Hartwell [5], and Blanton and Junkins [8].

As an alternative to recovery of the orbit simultaneously with the triangulation process, one can use tracking data to recover the orbit *a priori*, to within small clock biases, and often acceptable precision. The photomeasurements, in most cases will provide only marginal improvement in the orbit resolution due to the recent advances made in tracking systems for orbit determination. In any event, the triangulation should be dynamically constrained in the sense that the sequence of exposures lie along a dynamical path.

2.2 Rotational Dynamical Constraints

The incorporation of rotational dynamical constraints is, in concept, very analogous to introduction orbital constraints. The details, however, are somewhat more complicated. The direction cosines $C_{\ell m}$ contained in Equation (1) can be written as functions of three angles orienting the camera $\{c\}$ axes relative to the earth $\{e\}$ axes as

$$\{c\} = [C]\{e\} \quad (5)$$

where

$$[C] = \begin{bmatrix} c\psi_{ce} & s\psi_{ce} & 0 \\ -s\psi_{ce} & c\psi_{ce} & 0 \\ 0 & 0 & 1 \end{bmatrix} \begin{bmatrix} c\theta_{ce} & 0 & -s\theta_{ce} \\ 0 & 1 & 0 \\ s\theta_{ce} & 0 & c\theta_{ce} \end{bmatrix} \begin{bmatrix} 1 & 0 & 0 \\ 0 & c\phi_{ce} & s\phi_{ce} \\ 0 & -s\phi_{ce} & c\phi_{ce} \end{bmatrix} \quad (6)^*$$

This is the classical approach; each set of three orientation angles (for each of n exposures) are treated as n independent sets of three unknowns in the triangulation process.

Perhaps the most obvious approach (to introduce rotational dynamical constraints) is to derive a set of differential equations describing the $(\phi_{ce}, \theta_{ce}, \psi_{ce})$ angles and recover the six initial conditions (on these three angles and their first time derivatives) in lieu to treating the $3n$ angles as independent unknowns. Several factors should be considered, however. First, rotational dynamics is most naturally approached by viewing the motion from a non-rotating reference frame rather than an earth-fixed frame. Second, care should be taken to avoid the singularity that exists for certain orientations $[\theta_{ce} = \pm \pi/2, \text{ in Eqn. (6)}]$ for any choice of orientation angles. One should allow efficient advantage to be taken of on-board angular motion measurements (e.g. rate gyros, star sensors, sun sensors, etc.). In view of these considerations, we introduce (in lieu of $\phi_{ce}, \theta_{ce}, \psi_{ce}$) the angles $(\phi_{co}, \theta_{co}, \psi_{co})$ orienting the camera relative to an "orbiting" frame which maintains axes in the local radial, transverse, and normal directions so that (see Appendix 2)

$$[C] \equiv [CN] \equiv [CO][OO'] [O'N][EN]^T \quad (7)$$

where

$$[CO] = \begin{bmatrix} c\psi_{co} & s\psi_{co} & 0 \\ -s\psi_{co} & c\psi_{co} & 0 \\ 0 & 0 & 1 \end{bmatrix} \begin{bmatrix} c\theta_{co} & 0 & -s\theta_{co} \\ 0 & 1 & 0 \\ s\theta_{co} & 0 & c\theta_{co} \end{bmatrix} \begin{bmatrix} 1 & 0 & 0 \\ 0 & c\phi_{co} & s\phi_{co} \\ 0 & -s\phi_{co} & c\phi_{co} \end{bmatrix} \quad (8)$$

*For rotational compaction, we use "c" for "cosine" and "s" for "sine".

where

$I_{\alpha\beta}$ = spacecraft moments of inertia about mass center with axes oriented parallel to image plane axes.

$\{\omega_x, \omega_y, \omega_z\}$ = spacecraft angular velocity, components along camera image plane axes

$\{L_x, L_y, L_z\}$ = effective external torque acting on the spacecraft; components taken about mass center with axes parallel to camera image plane axes.

$$\begin{pmatrix} \omega_x \\ \omega_y \\ \omega_z \end{pmatrix} = [CG] \begin{pmatrix} \omega_{gx} \\ \omega_{gy} \\ \omega_{gz} \end{pmatrix}$$

$(\omega_{gx}, \omega_{gy}, \omega_{gz})$ = angular velocity components along rate gyro's three orthogonal axes.

$[CG]$ = assumed constant 3 x 3 interlock direction cosine matrix, orienting the camera axes with respect to the rate gyro axes.

In the event that the particular spacecraft departs significantly from the rigid body assumption (e.g., significant internal moving masses, vibration of flexible appendages), additional forcing terms will appear on the RHS of Eqn. (13), and one additional, coupled, differential equation for each such mechanical degree of freedom must be written. The kinematical Equation (13), however, holds rigorously for the motion of the camera axes, regardless of what torques are present and regardless of departures of the actual body model from the rigid body assumption. To employ Eqns. (12) as the starting point for modeling rotational dynamics requires excellent mathematical models for the actual torques (L_x, L_y, L_z) present and for any significant departures from the rigid body assumption. This viewpoint was pursued initially under this contract and yielded in the results published in References 7 and 8 (abstracted below in section 3.1).

The fact that Eqn. (13) is rigorously valid (regardless of the torque history and actual body flexibility) and since true angular velocity can be measured (by conventional rate gyros) motivates a *direct rate integration*

approach to imposing the rotational motion constraint. This approach leads one to consider the wisdom of bypassing the necessity of modeling the spacecraft flexibility and torque history by directly integrating Equations (13). This latter viewpoint has been investigated during this research project and does prove to be the most attractive option.

The orthogonal axes of the rate gyro package generally has some orientation other than the camera axes, thus we must account for the gyro-to-camera interlock rotation as

$$\begin{pmatrix} \omega_x \\ \omega_y \\ \omega_z \end{pmatrix} = [CG] \begin{pmatrix} \tilde{\omega}_{gx} \\ \tilde{\omega}_{gy} \\ \tilde{\omega}_{gz} \end{pmatrix} \quad (14)$$

where [CG] is a nominally constant, 3 x 3 interlock direction cosine matrix, and the measured angular rates are

$$\begin{pmatrix} \tilde{\omega}_{gx} \\ \tilde{\omega}_{gy} \\ \tilde{\omega}_{gz} \end{pmatrix} = \begin{pmatrix} \omega_{gx} \\ \omega_{gy} \\ \omega_{gz} \end{pmatrix} + \begin{pmatrix} b_x \\ b_y \\ b_z \end{pmatrix} + \begin{pmatrix} v_x \\ v_y \\ v_z \end{pmatrix} \quad (15)$$

$$\{\text{Measured}\} = \{\text{True}\} + \{\text{Bias}\} + \{\text{Measurement Noise}\}$$

If one substitutes the raw data $(\tilde{\omega}_{gx}, \tilde{\omega}_{gy}, \tilde{\omega}_{gz})$ through (14) directly into (13) and integrates to determine the angular rate history, the effects of the uncompensated rate biases $\{b_x, b_y, b_z\}$ and noise (v_x, v_y, v_z) will typically result in unacceptably rapid divergence of the integrated orientation history from the true orientation history. The results of numerical experimentation with typical noise levels (1 arc sec/sec) and bias values led us to conclude that the measured rates should be passed through a noise pre-filter (section 4) to obtain a filtered angular velocity history:

$$\frac{\partial}{\partial p_i} [C] = \left[\frac{\partial}{\partial p_i} [CO] \right] [00'] [0'N] [EN]^T \quad (18)$$

where we need

$$\begin{aligned} \frac{\partial}{\partial p_i} [CO] = & \frac{\partial \phi_{co}(t)}{\partial p_i} \begin{bmatrix} c\psi_{co} & s\psi_{co} & 0 \\ -s\psi_{co} & c\psi_{co} & 0 \\ 0 & 0 & 1 \end{bmatrix} \begin{bmatrix} c\theta_{co} & 0 & -s\theta_{co} \\ 0 & 1 & 0 \\ c\theta_{co} & 0 & c\theta_{co} \end{bmatrix} \begin{bmatrix} 0 & 0 & 0 \\ 0 & -s\phi_{co} & c\phi_{co} \\ 0 & -c\phi_{co} & -s\phi_{co} \end{bmatrix} \\ & + \frac{\partial \theta_{co}(t)}{\partial p_i} \begin{bmatrix} c\psi_{co} & s\psi_{co} & 0 \\ -s\psi_{co} & c\psi_{co} & 0 \\ 0 & 0 & 1 \end{bmatrix} \begin{bmatrix} -s\theta_{co} & 0 & -c\theta_{co} \\ 0 & 0 & 0 \\ c\theta_{co} & 0 & -s\theta_{co} \end{bmatrix} \begin{bmatrix} 1 & 0 & 0 \\ 0 & c\phi_{co} & s\phi_{co} \\ 0 & -s\phi_{co} & c\phi_{co} \end{bmatrix} \\ & + \frac{\partial \psi_{co}(t)}{\partial p_i} \begin{bmatrix} -s\psi_{co} & c\psi_{co} & 0 \\ -c\psi_{co} & -s\psi_{co} & 0 \\ 0 & 0 & 0 \end{bmatrix} \begin{bmatrix} c\theta_{co} & 0 & -s\theta_{co} \\ 0 & 1 & 0 \\ s\theta_{co} & 0 & c\theta_{co} \end{bmatrix} \begin{bmatrix} 1 & 0 & 0 \\ 0 & c\phi_{co} & s\phi_{co} \\ 0 & -s\phi_{co} & c\phi_{co} \end{bmatrix} \\ & i = 1, 2, 3, \dots, 6, \quad (19) \end{aligned}$$

The partials $\left[\frac{\partial [\phi_{co}(t), \theta_{co}(t), \psi_{co}(t)]}{\partial p_i} \right]$ are obtained by integrating the matrix differential equations

$$\dot{\Phi}(t, t_0) = F(t)\Phi(t, t_0) \quad , \quad \Phi(t_0, t_0) = \begin{bmatrix} 1 & 0 & 0 \\ 0 & 1 & 0 \\ 0 & 0 & 1 \end{bmatrix} \quad (20a)$$

and

$$\dot{\Psi}(t, t_0) = F(t)\Psi(t, t_0) + B(t) \quad , \quad \Psi(t_0, t_0) = [0] \quad (20b)$$

where

$$\Phi(t, t_0) \equiv \left[\frac{\partial [\phi_{co}(t), \theta_{co}(t), \psi_{co}(t)]}{\partial [\phi_{co}(t_0), \theta_{co}(t_0), \psi_{co}(t_0)]} \right] \quad (21a)$$

$$\Psi(t, t_0) \equiv \left[\frac{\partial [\phi_{co}(t_0), \theta_{co}(t), \psi_{co}(t)]}{\partial [b_1, b_2, b_3]} \right] \quad (21b)$$

$${}^{3 \times 3} [F(t)] = \frac{\partial [\text{right hand side of Eqns. (17)}]}{\partial [\phi_{co}(t), \theta_{co}(t), \psi_{co}(t)]} \quad (22a)$$

$${}^{3 \times 3} [B(t)] = \frac{\partial [\text{right hand side of Eqns. (17)}]}{\partial [b_1, b_2, b_3]} \quad (22b)$$

The partials (22) are taken by direct differentiation of Equations (17).

2.4 OBSERVATION EQUATIONS FOR DYNAMICALLY CONSTRAINED PHOTOGRAMMETRIC ADJUSTMENTS

2.4.1 Basic Notations

Linearization of the collinearity equations (1) leads to the matrix equation*

$$\Delta Y = A \Delta X + E \quad (23)$$

where ΔY = $m \times 1$ matrix of "measured minus computed" residuals of $x_{p_{ij}}$, $y_{p_{ij}}$ or

$$\{\Delta Y\} = \begin{pmatrix} \Delta x_{p_{11}} \\ \Delta y_{p_{11}} \\ \Delta x_{p_{21}} \\ \Delta y_{p_{21}} \\ \vdots \\ \vdots \\ \vdots \\ \Delta x_{p_{ij}} \\ \Delta y_{p_{ij}} \\ \vdots \\ \vdots \\ \vdots \end{pmatrix} \quad (24)$$

$[A] = \left[\frac{\partial Y}{\partial X} \right] = m \times n$ matrix ($m > n$) of partial derivatives of the $(x_{p_{ij}}, y_{p_{ij}})$ with respect to the elements of the vector $\{X\}$ of unknown parameters, evaluated with the current best estimates of X . (25)

$\{\Delta X\}$ = an $n \times 1$ matrix of desired corrections to the parameter vector $\{X\}$

$\{E\} = \Delta Y - A \Delta X$ = an $m \times 1$ matrix of "errors after the solution" associated with any choice for ΔX . (26)

* Subscript ij denotes i th point measured on the j th photograph.

The least squares solution for Δx minimizes $E^T W E$ and is well known to be the normal equations $\Delta X = (A^T W A)^{-1} A^T W \Delta Y$ where W is a positive definite weight matrix.

For traditional (unconstrained) photogrammetric adjustments, the $\{X\}$ vector can be partitioned as

$$\{X\} = \begin{Bmatrix} \{XYZC\} \\ \{ \phi \theta \psi \} \\ \{XYZP\} \end{Bmatrix} \quad (27)$$

where

$$\{XYZC\} = \begin{Bmatrix} X_{c1} \\ Y_{c1} \\ Z_{c1} \\ \vdots \\ X_{cj} \\ Y_{cj} \\ Z_{cj} \\ \vdots \end{Bmatrix} = \text{matrix of camera exposure stations' coordinates} \quad (28)$$

$$\{ \phi \theta \psi \} = \begin{Bmatrix} \phi_1 \\ \theta_1 \\ \psi_1 \\ \vdots \\ \phi_j \\ \theta_j \\ \psi_j \end{Bmatrix} = \text{matrix of "1-2-3" camera orientation angles (depending upon the option used, these may relate camera axes to the instantaneous radial transverse, and normal directions; or directly to the earth-fixed axes).} \quad (29)$$

$$\{XYZP\} = \begin{Bmatrix} X_{p_1} \\ Y_{p_1} \\ Z_{p_1} \\ \vdots \\ X_{p_i} \\ Y_{p_i} \\ Z_{p_i} \\ \vdots \end{Bmatrix} = \text{matrix of pass points' coordinates} \quad (30)$$

and the matrix of partial derivatives can be similarly partitioned as

$$[A] = [[XYZC] [A\phi\theta\psi] [XYZP]] \quad (31)$$

where the submatrices are

$$[XYZC] = \left[\frac{\partial(X_{p_{11}}, Y_{p_{11}}, X_{p_{21}}, Y_{p_{21}}; \dots; X_{p_{ij}}, Y_{p_{ij}}; \dots)}{\partial(X_{c_1}, Y_{c_1}, Z_{c_1}; X_{c_2}, Y_{c_2}, Z_{c_2}; \dots; X_{c_j}, Y_{c_j}, Z_{c_j}; \dots)} \right] \quad (32)$$

$$[A\phi\theta\psi] = \left[\frac{\partial(X_{p_{11}}, Y_{p_{11}}; X_{p_{21}}, Y_{p_{21}}; \dots; X_{p_{ij}}, Y_{p_{ij}}; \dots)}{\partial(\phi_1, \theta_1, \psi_1; \phi_2, \theta_2, \psi_2; \dots; \phi_j, \theta_j, \psi_j; \dots)} \right] \quad (33)$$

and

$$[XYZP] = \left[\frac{\partial(X_{p_{11}}, Y_{p_{11}}; X_{p_{21}}, Y_{p_{21}}; \dots; X_{p_{ij}}, Y_{p_{ij}}; \dots)}{\partial(X_{p_1}, Y_{p_1}, Z_{p_1}; X_{p_2}, Y_{p_2}, Z_{p_2}; \dots; X_{p_i}, Y_{p_i}, Z_{p_i}; \dots)} \right] \quad (34)$$

If one introduces translational dynamical constraints, then (for a single strip of photographs and using the simplifying assumption that the n exposure times are perfectly measurable) the $\{X\}$ vector (27) and A matrix (31) become

$$\{X\} = \begin{Bmatrix} \{OE\} \\ \{A\phi\theta\psi\} \\ \{XYZP\} \end{Bmatrix} \quad (35)$$

and

$$[A] = [[AOE] [A\phi\theta\psi] [AXYZP]] \quad (36)$$

where

$$OE = \begin{pmatrix} OE_1 \\ OE_2 \\ \vdots \\ OE_6 \end{pmatrix} = \text{a set of six orbit elements defining the best fitting orbit (for example, the initial orbit state vector } (X_o, Y_o, Z_o, \dot{X}_o, \dot{Y}_o, \dot{Z}_o) \text{).} \quad (37)$$

and

$$[AOE] = \left[\frac{\partial (X_{P11}, Y_{P11}; X_{P21}, Y_{P21}; \dots; X_{Pij}, Y_{Pij}; \dots)}{\partial (OE_1, OE_2, \dots, OE_6)} \right] \quad (38)$$

If one introduces both translational and rotational dynamical constraints, then (again, for a single strip of photographs), the $\{X\}$ vector (27,35) and the A matrix (31,36) become

$$\{X\} = \begin{pmatrix} \{OE\} \\ \{AE\} \\ \{XYZP\} \end{pmatrix} \quad (39)$$

and

$$[A] = [[AOE] [AAE] [AXYZP]] \quad (40)$$

where

$$\{AE\} = \begin{pmatrix} AE_1 \\ AE_2 \\ \vdots \\ AE_6 \end{pmatrix} = \text{a set of six attitude elements defining the best fitting attitude solution (for example, the initial orientation state vector, } \phi_o, \theta_o, \psi_o, b_1, b_2, b_3 \text{)}$$

and

$$[AAE] = \left[\frac{\partial (X_{P11}, Y_{P11}; X_{P21}, Y_{P21}; \dots; X_{Pij}, Y_{Pij}; \dots)}{\partial (AE_1, AE_2, \dots, AE_6)} \right] \quad (41)$$

The above symbology may prove difficult to extrapolate to specific situations, we therefore provide a simple prototype adjustment problem

as an illustration. It will also be evident that multiple strip (block) adjustment present no particular difficulties; independent dynamical constraints are introduced for each strip of photography.

2.4.2 An Example Adjustment Problem Setup

Referring to Figure 3, an idealized block adjustment of 2 strips containing 5 photographs each is considered. Six complete ground control points are indicated by ".", 19 pass points are located at each "." and under each photo's principal point ("+"). Thus, in this idealized adjustment problem, each of the ten photographs has at least one control point; photos 2, 3, 4, 7, 8, and 9 have a total of 9 measurable points (108 measurements), while photos 1, 5, 6 and 10 have 6 measurable points (48 measurements).

We first consider the classical approach in which no dynamical constraints are imposed. The total number of equations (one for each measurement) is

$$\begin{aligned} 2 \sum_{j=1}^{\# \text{ of photos}} [\text{measurable points in photography}] &= 2[6+9+9+9+6+6+9+9+9+6] \\ &= 156 \end{aligned} \quad (42)$$

The number of unknowns associated with the 19 pass points is

$$\# \text{ of elements in } \{XYZP\} = 3 \times 19 = 57 \quad (43)$$

The number of unknown camera exposure station coordinates is

$$\# \text{ of elements in } \{XYZC\} = 3 \times 10 = 30 \quad (44)$$

The number of unknown orientation coordinates is

$$\# \text{ of elements in } \{\phi\theta\psi\} = 3 \times 10 = 30 \quad (45)$$

Therefore, the total number of unknowns (without dynamical constraints) is $57 + 30 + 30 = 117$.

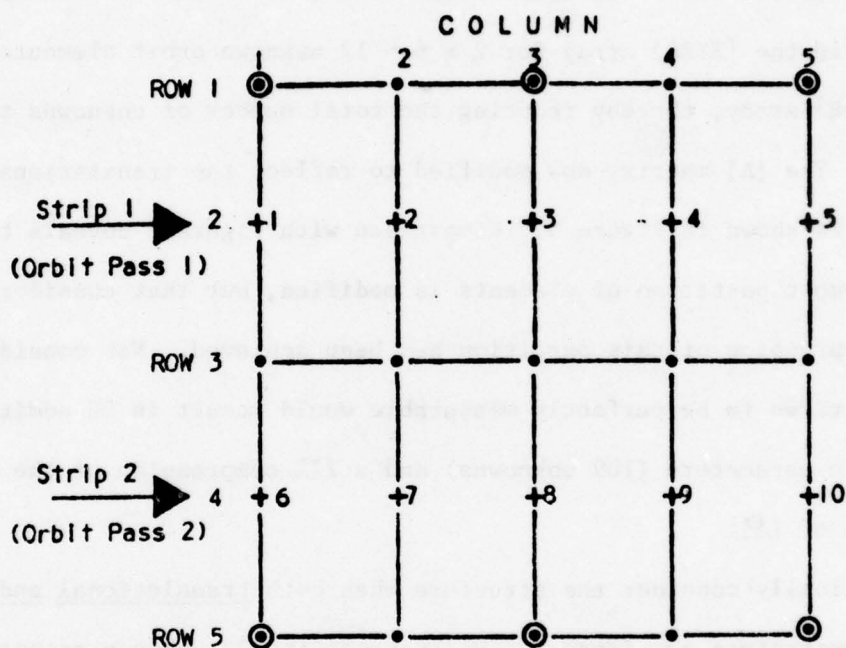


Fig. 3 An Example Triangulation Block of 2 Strips of 5 Photographs Each (6 complete ground control points are denoted by \odot , the 10 camera exposure points are indicated by +, 19 pass points are located at the \cdot and + symbols, 50% overlap is assumed along each strip)

The structure of the [A] matrix for this example (without constraints) is graphically illustrated in Figure 4. The left, middle, and right partitions of Figure 2 correspond identically to the partitions of Equation (35). The shaded areas are the nonzero entries.

We now consider the changes which occur in the structure of the partial derivative matrix when translation (orbital) constraints are incorporated. Since two orbital arcs are present, then one dynamical (best fitting) solution will be recovered for each strip. Thus, we "trade" the 30 unknown elements in the {XYZC} array for $2 \times 6 = 12$ unknown orbit elements in a 12×1 {OE} array, thereby reducing the total number of unknowns to $117 - 18 = 99$. The [A] matrix, now modified to reflect the translational constraints is shown in Figure 5. Comparison with Figure 2 reveals that only the left-most partition of elements is modified, but that considerable (60%) compression of this partition has been achieved. Not considering exposure times to be perfectly measurable would result in 10 additional adjustable parameters (109 unknowns) and a 27% compression of the first partition of [A].

We finally consider the structure when both translational and rotational constraints are imposed. We exchange the 30 unknown orientation parameters for $2 \times 6 = 12$ unknown orientation elements (1 set of six for each of the 2 strips). The [A] matrix, sketched in Figure 6 now shows a 60% compression of the center partition (the total number of unknowns is now $117 - 36 = 81$). This 60% compression of the center partition is achieved even if one must also recover the n exposure times, since these times would have already been included in incorporating the orbital constraints. In practice, however, the quality of the gyro data and auxiliary attitude measurements will dictate whether or not this theoretical truth results in improved or degraded precision. The simulations

PHOTO #	POINT #	CAMERA EXPOSURE COORDINATES' PARTIALS	CAMERA ORIENTATION ANGLES' PARTIALS	PARTIAL DERIVATIVES OF THE PASS POINTS' COORDINATES (2 x 3 SUB-MATRICES)																					
				12	14	21	22	23	24	31	32	33	34	41	42	43	44	51	52	53	54	61	62	63	64
1	11																								
	12																								
	21																								
	22																								
	31																								
2	13																								
	14																								
	21																								
	22																								
	31																								
3	13																								
	14																								
	21																								
	22																								
	31																								
4	13																								
	14																								
	21																								
	22																								
	31																								
5	13																								
	14																								
	21																								
	22																								
	31																								
6	13																								
	14																								
	21																								
	22																								
	31																								
7	13																								
	14																								
	21																								
	22																								
	31																								
8	13																								
	14																								
	21																								
	22																								
	31																								
9	13																								
	14																								
	21																								
	22																								
	31																								
10	13																								
	14																								
	21																								
	22																								
	31																								

Fig. 4 Partial Derivative Matrix [A] for Observation Equations for the 2 Strip Block of Fig. 3

NO DYNAMICAL CONSTRAINTS

PHOTO #	POINT #	PARTIALS W.R.T. ORBIT 1 ORBIT ELEMENTS	PARTIALS W.R.T. ORBIT 2 ORBIT ELEMENTS	CAMERA ORIENTATION ANGLES' PARTIALS	PARTIAL DERIVATIVES OF THE PASS POINTS' COORDINATES (2 x 3 SUB-MATRICES)																																																																																																																																																																																																																																																																																																																																																																																																																																																																																																																																																																																																																																																																																																																																																																																																																																																																																																																																																																																																																																																																																																																																																																																																																																																																																																																																																																										
					12	14	21	22	23	24	26	31	32	33	34	35	41	42	43	44	45	52	54																																																																																																																																																																																																																																																																																																																																																																																																																																																																																																																																																																																																																																																																																																																																																																																																																																																																																																																																																																																																																																																																																																																																																																																																																																																																																																																																																								

Fig. 5 Partial Derivative Matrix [A] for Observation Equations for the 2 Strip Block for Fig. 3 WITH TRANSLATIONAL DYNAMICAL CONSTRAINTS

PHOTO #	POINT #	PARTIALS W.R.T. ORBIT 1 ORBIT ELEMENTS	PARTIALS W.R.T. ORBIT 2 ORBIT ELEMENTS	PARTIALS W.R.T. ORBIT 1 ATTITUDE ELEMENTS	PARTIALS W.R.T. ORBIT 2 ATTITUDE ELEMENTS	PARTIAL DERIVATIVES OF THE PASS POINTS' COORDINATES (2 x 3 SUB-MATRICES)																															
						18	14	21	22	23	24	25	26	31	32	33	34	35	41	42	43	44	45	52	54												
1	1	1	1	1	1	1	1	1	1	1	1	1	1	1	1	1	1	1	1	1	1	1	1	1	1	1											
	2	1	1	1	1	1	1	1	1	1	1	1	1	1	1	1	1	1	1	1	1	1	1	1	1	1											
	3	1	1	1	1	1	1	1	1	1	1	1	1	1	1	1	1	1	1	1	1	1	1	1	1	1											
2	1	1	1	1	1	1	1	1	1	1	1	1	1	1	1	1	1	1	1	1	1	1	1	1	1	1											
	2	1	1	1	1	1	1	1	1	1	1	1	1	1	1	1	1	1	1	1	1	1	1	1	1	1											
	3	1	1	1	1	1	1	1	1	1	1	1	1	1	1	1	1	1	1	1	1	1	1	1	1	1											
3	1	1	1	1	1	1	1	1	1	1	1	1	1	1	1	1	1	1	1	1	1	1	1	1	1	1											
	2	1	1	1	1	1	1	1	1	1	1	1	1	1	1	1	1	1	1	1	1	1	1	1	1	1											
	3	1	1	1	1	1	1	1	1	1	1	1	1	1	1	1	1	1	1	1	1	1	1	1	1	1											
4	1	1	1	1	1	1	1	1	1	1	1	1	1	1	1	1	1	1	1	1	1	1	1	1	1	1											
	2	1	1	1	1	1	1	1	1	1	1	1	1	1	1	1	1	1	1	1	1	1	1	1	1	1											
	3	1	1	1	1	1	1	1	1	1	1	1	1	1	1	1	1	1	1	1	1	1	1	1	1	1											
5	1	1	1	1	1	1	1	1	1	1	1	1	1	1	1	1	1	1	1	1	1	1	1	1	1	1											
	2	1	1	1	1	1	1	1	1	1	1	1	1	1	1	1	1	1	1	1	1	1	1	1	1	1											
	3	1	1	1	1	1	1	1	1	1	1	1	1	1	1	1	1	1	1	1	1	1	1	1	1	1											
6	1	1	1	1	1	1	1	1	1	1	1	1	1	1	1	1	1	1	1	1	1	1	1	1	1	1											
	2	1	1	1	1	1	1	1	1	1	1	1	1	1	1	1	1	1	1	1	1	1	1	1	1	1											
	3	1	1	1	1	1	1	1	1	1	1	1	1	1	1	1	1	1	1	1	1	1	1	1	1	1											
7	1	1	1	1	1	1	1	1	1	1	1	1	1	1	1	1	1	1	1	1	1	1	1	1	1	1											
	2	1	1	1	1	1	1	1	1	1	1	1	1	1	1	1	1	1	1	1	1	1	1	1	1	1											
	3	1	1	1	1	1	1	1	1	1	1	1	1	1	1	1	1	1	1	1	1	1	1	1	1	1											
8	1	1	1	1	1	1	1	1	1	1	1	1	1	1	1	1	1	1	1	1	1	1	1	1	1	1											
	2	1	1	1	1	1	1	1	1	1	1	1	1	1	1	1	1	1	1	1	1	1	1	1	1	1											
	3	1	1	1	1	1	1	1	1	1	1	1	1	1	1	1	1	1	1	1	1	1	1	1	1	1											
9	1	1	1	1	1	1	1	1	1	1	1	1	1	1	1	1	1	1	1	1	1	1	1	1	1	1											
	2	1	1	1	1	1	1	1	1	1	1	1	1	1	1	1	1	1	1	1	1	1	1	1	1	1											
	3	1	1	1	1	1	1	1	1	1	1	1	1	1	1	1	1	1	1	1	1	1	1	1	1	1											
10	1	1	1	1	1	1	1	1	1	1	1	1	1	1	1	1	1	1	1	1	1	1	1	1	1	1											
	2	1	1	1	1	1	1	1	1	1	1	1	1	1	1	1	1	1	1	1	1	1	1	1	1	1											
	3	1	1	1	1	1	1	1	1	1	1	1	1	1	1	1	1	1	1	1	1	1	1	1	1	1											

Fig. 6 Partial Derivative Matrix [A] for
Observation Equations for the 2
Strip Block of Fig. 3
WITH TRANSLATIONAL AND ROTATIONAL DYNAMICAL
CONSTRAINTS

make a weak case for increased accuracy, but a strong case for increased computational efficiency.

2.5 Sequential (Kalman Filter) Approach to Dynamically Constrained Triangulation

2.5.1 The Extended Kalman Filter Algorithm

Given a system described by nonlinear equations of the form

$$\dot{X} = F(t, X) + V_x \quad (42)$$

with measurements modeled by

$$Y = G(X) + V_y \quad (43)$$

where V_x and V_y are Gaussian noise vectors with zero mean; it is assumed V_x and V_y are uncorrelated.

If a sequence of measurements are available

$$\{t_1, Y_1, t_2, Y_2, \dots, t_k, Y_k, \dots\}$$

Then the extended Kalman estimation algorithm (see ref. 10) is defined by the recursions

$$\hat{X}_{k+1}(t_{k+1}) = \bar{X}_k(t_{k+1}) + K(t_{k+1}) [Y_{k+1} - G(\bar{X}_k(t_{k+1}))] \quad (44a)^*$$

where

$$\bar{X}_k(t_{k+1}) = \text{forward *nonlinear* integration of Equation (42) from } \hat{X}_k(t_k)$$

$$K(t_{k+1}) = P_k(t_{k+1}) H^T(t_{k+1}) [\Lambda_{v_{k+1}v_{k+1}} + H(t_{k+1}) P(t_{k+1}) H^T(t_{k+1})]^{-1} \quad (44b)$$

= Kalman Gain Matrix

$$P_j(t_{k+1}) = \Phi(t_{k+1}, t_k) P_k(t_k) \Phi^T(t_{k+1}, t_k) + Q \quad (44c)$$

$$P_{k+1}(t_{k+1}) = X - \text{covariance matrix} = [I - K(t_{k+1}) H(t_{k+1})] P_k(t_{k+1}) \quad (44d)$$

$$H \equiv \left[\frac{\partial G}{\partial X} \right] = \text{partials of the measured variables with respect to the state vector} \quad (44e)$$

$$\Phi(t, t_k) = \text{nxn state transition matrix, the solution of the differential equation}$$

$$\dot{\Phi}(t, t_k) = \left[\frac{\partial F}{\partial X} \right] \Phi(t, t_k); \Phi(t_k, t_k) = I \quad (44f)$$

* Interpretation of subscripts: $\hat{X}_j(t_k)$ = "the best estimate of X at time t_k based upon the first j data subsets".

Q = process noise covariance matrix variance of x - vector due to the presence of the noise vector V_x in Equation (42).

2.5.2 Particularization of the Extended Kalman Estimation Algorithm to the Constrained Triangulation Problem

The above algorithm can be applied to the constrained triangulation problem by making the following definitions:

$$X = \text{state vector} = \begin{Bmatrix} \{OE\} \\ \text{---} \\ \{AE\} \\ \text{---} \\ \{XYZP\} \end{Bmatrix} = \begin{Bmatrix} X \\ Y \\ Z \\ \vdots \\ \dot{X} \\ \dot{Y} \\ \dot{Z} \\ \dots \\ \phi \\ \theta \\ \psi \\ b^x \\ b^y \\ b^z \\ \dots \\ \{XYZP\} \end{Bmatrix} \quad (45)$$

then

$$F \equiv \frac{dX}{dt} = \begin{Bmatrix} \{F\} \\ \{F^{oe}\} \\ \{0^{ae}\} \end{Bmatrix} \quad (46a)$$

with

$$\{F^{oe}\} = \begin{Bmatrix} \dot{X} \\ \dot{Y} \\ \dot{Z} \\ -\mu x/r^3 + \text{x-perturbation} \\ -\mu y/r^3 + \text{y-perturbation} \\ -\mu z/r^3 + \text{z-perturbation} \end{Bmatrix} \quad (46b)$$

$$\{F^{ae}\} = \begin{Bmatrix} \phi \\ \theta \\ \psi \\ \text{---} \\ 0 \\ 0 \\ 0 \end{Bmatrix} \quad (46c)$$

$$\begin{Bmatrix} \dot{\phi} \\ \dot{\theta} \\ \dot{\psi} \end{Bmatrix} = \text{Equation (17)}$$

Y_k = the kth particular set of measured image coordinates
of images appearing in the kth photograph

$$\begin{pmatrix} x_1 \\ y_1 \\ x_2 \\ y_2 \\ \vdots \end{pmatrix}_k \quad (47)$$

$H(t_k)$ = all pairs of Equations (1), one pair corresponding to each
image measured in the kth photograph.

$$\begin{aligned} \left\{ \frac{\partial H}{\partial X} \right\} &= \left[\frac{\partial H}{\partial(x,y,z)} \quad \frac{\partial H}{\partial(x,y,z)} \quad \frac{\partial H}{\partial(\phi,\theta,\psi)} \quad \frac{\partial H}{\partial(bx,by,bz)} \quad \frac{\partial H}{\partial(XYZP)} \right] \\ &= \left[\frac{\partial H}{\partial(x,y,z)} \quad 0 \quad \frac{\partial H}{\partial(\phi,\theta,\psi)} \quad 0 \quad \frac{\partial H}{\partial(XYZP)} \right] \end{aligned} \quad (48)$$

$\left[\frac{\partial H}{\partial(X,Y,Z)} \right]$ = partials of Equations (1) w.r.t. (X_c, Y_c, Z_c)

$\left[\frac{\partial H}{\partial(\phi,\theta,\psi)} \right]$ = partials of Equations (1) w.r.t. (ϕ, θ, ψ)

$\left[\frac{\partial H}{\partial(XYZP)} \right]$ = partials of equations (1) w.r.t. (X_p, Y_p, Z_p)

$$\left[\frac{\partial F}{\partial X} \right] = \frac{\partial \begin{Bmatrix} \{F_{oe}\} \\ \{F_{ae}\} \\ \{0\} \end{Bmatrix}}{\partial \begin{Bmatrix} \{OE\} \\ \{AE\} \\ \{XYZP\} \end{Bmatrix}} = \begin{bmatrix} \frac{\partial \{F_{oe}\}}{\partial \{OE\}} & \frac{\partial \{F_{oe}\}}{\partial \{AE\}} & 0 \\ \frac{\partial \{F_{ae}\}}{\partial \{OE\}} & \frac{\partial \{F_{ae}\}}{\partial \{AE\}} & 0 \\ 0 & 0 & 0 \end{bmatrix} \quad (49a)$$

$$\left[\frac{\partial \{F_{oe}\}}{\partial \{OE\}} \right] = \begin{bmatrix} 6 \times 6 & 3 \times 3 & 3 \times 3 \\ 0 & I & \\ G & 0 & \end{bmatrix} \quad (49b)$$

$$[G] = \frac{3}{r^5} \begin{bmatrix} (X^2 - r^2/3) & XY & YZ \\ XY & (Y^2 - r^2/e) & YZ \\ XZ & YZ & (r^2 - r^2/3) \end{bmatrix} + \text{orbital perturbations} \quad (49c)$$

$$\frac{\partial \{F_{oe}\}}{\partial \{AE\}} = 0 \quad [\text{zero unless orbital perturbations which depend upon attitude drag, are included in the force model}]$$

$$\frac{\partial \{F_{ae}\}}{\partial \{OE\}} = [0] + \text{perturbations}$$

$$\left[\frac{\partial \{F_{ae}\}}{\partial \{AE\}} \right] = \left[\frac{\partial (\dot{\phi}, \dot{\theta}, \dot{\psi}, \dot{b}_x, \dot{b}_y, \dot{b}_z)}{\partial (\phi, \theta, \psi, b_x, b_y, b_z)} \right] = \begin{bmatrix} \frac{\partial (\dot{\phi}, \dot{\theta}, \dot{\psi})}{\partial (\phi, \theta, \psi)} & \frac{\partial (\dot{\phi}, \dot{\theta}, \dot{\psi})}{\partial (b_x, b_y, b_z)} \\ 0 & 0 \end{bmatrix} \quad (49d)$$

$$\left[\frac{\partial (\dot{\phi}, \dot{\theta}, \dot{\psi})}{\partial (\phi, \theta, \psi)} \right] = \text{partials of Equations (17), w.r.t. } (\phi, \theta, \psi)$$

$$\left[\frac{\partial (\dot{\phi}, \dot{\theta}, \dot{\psi})}{\partial (b_x, b_y, b_z)} \right] = \text{partials of Equations (17), w.r.t., } (b_x, b_y, b_z)$$

$$Q = \begin{bmatrix} Q_0 & & 0 \\ & Q_A & \\ 0 & & Q_{XYZP} \end{bmatrix} = \text{Process Noise Matrix} \quad (50a)$$

$$6 \times 6 \\ Q_0 = 0$$

$$6 \times 6 \\ Q_A = \sigma_{\text{gyro}}^2 \begin{bmatrix} 1 & 0 \\ 0 & 1 \end{bmatrix} \quad (50b)$$

$$Q_{XYZP} = 0$$

The above algorithm is applied to a dynamically constrained triangulation problem in section 4.0.

It should be noted that the {XYZP} vector includes only the particular coordinates of the points measured on the $k + 1^{\text{th}}$ photograph; thus the computer program requires careful "bookkeeping" which dynamically alters this array and the associated matrices in the Kalman filter algorithm to remain consistent with the $(k + 1)^{\text{th}}$ set of elements of {XYZP}.

The Kalman algorithm convergence history (ref. 10) leads to the conclusion that the above algorithm should be iterated through all measurements at least two or three times to obtain the best estimates. In the absence of process noise (from gyro measurements), Junkins (10) has demonstrated numerical equivalence between the iterated Kalman algorithm and the batch least squares algorithm. The presence of process noise, however, precludes a rigorous application of the batch least squares algorithm and thereby leaves the sequential Kalman algorithm as the only practical alternative.

3.0 BATCH TRIANGULATION EXAMPLES

3.1 Example 1: Torque-Free Case

In this example, we consider an uncontrolled satellite moving in a 100 mile circular orbit. Two-body orbital dynamics are assumed. The rotational dynamics is assumed governed by Equations (12) and (13) with $L_x = L_y = L_z = 0$ (i.e., a rigid spacecraft, subject to zero external torque). Equations (12) and (13) have analytical solutions for this case, and analytical solutions for all required partial derivatives have been derived (see Ref. 7 and 8). For purposes of illustration, a short strip of photography was simulated; corresponding to four photographs made by a camera fixed in a rigid triaxial satellite from a 100 mile circular orbit. Two-body translational motion and torque-free rotational motion were assumed. A single strip of four photographs, each with approximately 50% overlap was generated. These photographs covered a ground strip of approximately 100 miles by 250 miles.

Four control points and eight pass points were chosen on the ground strip and distributed in such a fashion as to give a total of 60 observation equations. The image coordinates were modified to simulate 1 mil measurement precision. It was further assumed that the camera focal length, f , the principal point offset (x_o, y_o) and the camera exposure times were perfectly known. Initial guesses of the pass point coordinates and camera center coordinates were corrupted from their true values by an average of 2 miles. Initial guesses on camera axes Euler angles were corrupted by an average of 1.5° .

Three separate least squares differential correction programs were written to illustrate the impact of dynamical constraints:

UCPHOTO (unconstrained photogrammetry): all parameters appearing in the observation equations were treated as independent. The dimensions

of the A matrix* were 60 (observations) x 48 (parameters), where
48 = 3 times the number of pass points plus 3 times the number of camera
center locations plus 3 camera axes Euler angles at each exposure time
= 3(8) + 3(4) + 3(4).

OCPHOTO (orbit constrained photogrammetry): pass point coordinates, camera
orientation at each time and orbit initial conditions were considered
independent. The A matrix was dimensioned 60 (observations) x 42
(parameters), where 42 = 3 times the number of pass points plus 6 orbit
initial conditions plus 3 Euler angles for each photograph = 3(8) + 6 +
3(4).

DCPHOTO (fully dynamically constrained photogrammetry): pass point
coordinates, orbit initial conditions and attitude initial conditions
were considered independent. The dimensions of the A matrix were 60
(observations) x 36 (parameters) where 36 = 3 times the number of pass
points plus 6 orbit initial conditions plus 6 attitude initial conditions
= 3(8) + 6 + 6.

The structure of the A matrix for these three cases is shown in
Figures 7a, 7b, and 7c, respectively. The shaded region contains the non-
zero elements. The essential results of these numerical tests were
summarized in Table 1. For this simple problem the best results were
obtained using full dynamical constraints. (Even though the dimension
of the A matrix was reduced from 60 x 48 to 60 x 36, the computer run
time was not decreased). This is because the matrix inversion savings
were offset by the relatively elaborate dynamical model. The matrix
calculations, however, dominate real world triangulation problems.
Consequently, substantial cost reductions may be achieved in practical
applications.

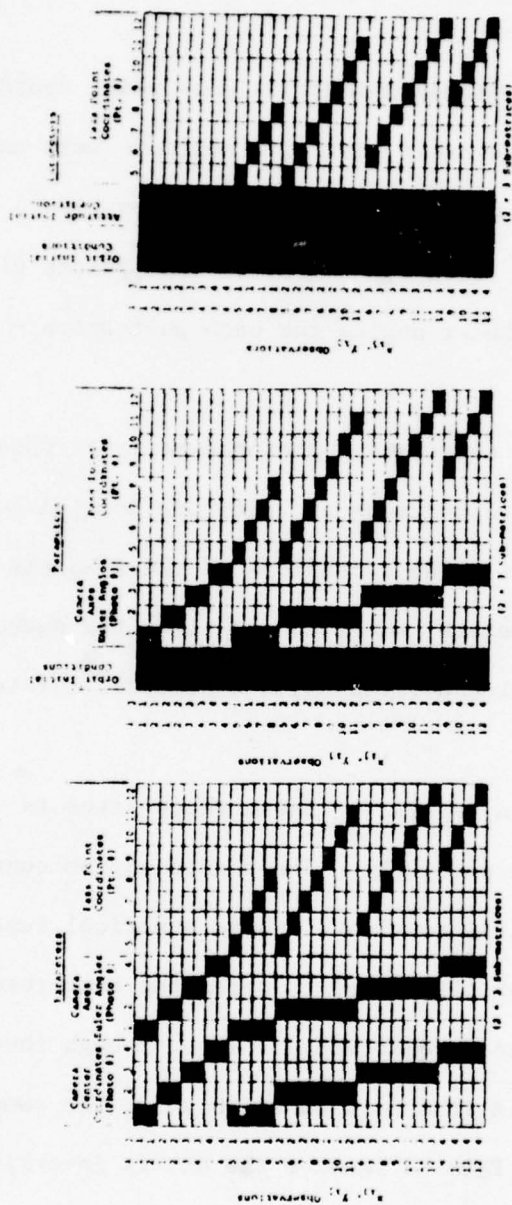


Fig. 7a No Dynamical Constraints

Fig. 7b Orbit Dynamical Constraints

Fig. 7c Fully Dynamical Constraints

Fig. 7 Structure of the A matrix $\frac{3(\text{measurements})}{3(\text{unknown parameters})}$ for Unconstrained, Orbit constrained and Attitude constrained Triangulation of Orbital Photography

Program	Max pass pt error after convergence (true - converged) (ft)	Mean pass point error (ft)	Std. dev. of all errors (ft)	CDC 6400 central processor time (sec)
UCPHOTO	205.08	12.24	73.58	5.82
OCPHOTO	93.45	-6.36	37.47	5.66
DCPHOTO	-57.88	-1.60	25.54	6.86

Table 1 A comparison of the effects of dynamical constraints on photogrammetric triangulation.

3.2 Example 2: A 10 Photo Strip (Via Batch Least Squares Triangulation)

This example is similar to the DC Photo example above, except in two respects: (1) instead of assuming zero torque and using the analytical solution of Ref. 7, the Euler differential equations were integrated with the true torque history specified, (2) the number of photos in the strip was increased from 4 to 10 to provide more realistic dimensions for the demonstration.

138 simulated measurements were calculated for a total of 69 photographic images of 10 control points and 25 pass points. The simulated measurement errors were initially set to zero to verify that the converged solutions (from a wide variety of starting estimates) recovered true angles and position coordinates to acceptable precision (all angles were recovered to within 1 arc sec and all camera and pass point coordinates recovered to within .15 ft.). In particular, Tables 2 and 3 summarize the pass point coordinates' starting estimates, converged values, and true minus converged residuals in miles; analogous results are recorded in Table 3 for the orbit and attitude state variables. This example required approximately one minute of central processor run time, over half of which was spent manipulating and inverting matrices (as opposed to integrating the equations of motion).

This example, albeit for an idealized case, demonstrates clearly the validity of the dynamically constrained approach for the case that the actual torque history can be accurately modeled. However, this restriction, along with the rigid satellite assumption are, in fact, major obstacles in practical applications. To circumvent the necessity of modeling torques and making idealizing assumptions regarding satellite rigidity, we incorporate angular rate gyro measurements. The availability of angular rate measurements permits the luxury of not modeling torques or body flexibility [in order to correctly generalize Equations (12)], rather, one directly integrates Equation (17). This approach leads to two algorithms (batch and sequential), which are applied to example cases below.

TABLE 2
Batch Least Squares
Pass Point Solution Summary for Example 2

Point Number		Starting Value (miles)	Converged Value (miles)	Converged Minus True Residual (ft)
1	x	1.000000	0.000004	+0.02
	y	10.500000	10.000006	+0.03
	z	3962.400000	3963.399997	-0.02
2	x	-37.000000	-38.999998	+0.01
	y	40.000000	39.000004	+0.02
	z	3962.000000	3963.000002	+0.01
3	x	-12.000000	-10.000004	-0.02
	y	42.000000	41.999995	-0.03
	z	3962.000000	3962.500025	+0.13
25
	x	44.000000	45.000004	+ .02
	y	431.000000	429.999995	- .03
	z	3941.000000	3940.49981	- .10

Notes on error statistics:

- Mean error (over all 25 pass points) \approx .0001 ft.
- RMS error (over all 25 pass points) \approx 0.05 ft.
- Convergence was achieved from the starting values shown in 4 differential corrections.
- For brevity, only 4 of the twenty-five pass point coordinates are shown.
- Since perfect measured values were used in this example, the above small residuals simply reflect the fact that (a) the algorithm has been correctly implemented, and (b) adequate precision and convergence tolerances were employed.

TABLE 3
Batch Solution Summary for Initial Orbit and Attitude
State Variables (Example 2)

	Starting Value	Converged Value	Converged Minus True Residual
x_o	0.004200 miles	0.003801 miles	.005 ft.
y_o	0.002700 miles	0.000702 miles	.01 ft.
z_o	4062.181900 miles	4063.181898 miles	-.01 ft.
\dot{x}_o	-0.000160 miles/sec	-0.000060 miles/sec	.00 ft/sec.
\dot{y}_o	4.911200 miles/sec	4.851200 miles/sec	.00 ft/sec.
\dot{z}_o	-0.000100 miles/sec	-0.000160 miles/sec	.00 ft/sec.
ϕ_o	-0.000042 rad.	-0.000020 rad.	+1.0 arc sec
θ_o	0.000100 rad.	0.000000 rad.	0.0 arc sec
ψ_o	0.000028 rad.	0.000030 rad.	-0.9 arc sec
$\dot{\phi}_o$	-0.002100 rad/sec	-0.001100 rad/sec	0.00 rad/sec
$\dot{\theta}_o$	0.000150 rad/sec	0.000100 rad/sec	0.00 rad/sec
$\dot{\psi}_o$	0.000910 rad/sec	0.000990 rad/sec	-0.00 rad/sec

Notes:

These values correspond to the same converged solution (after 4 corrections) as the pass point summary of Table 2.

3.3 Example 3: A Batch Estimation Example Using the *Direct Rate Integration Approach*

This example is very similar to example 2, except the rotational dynamical model consists of equation (17) [instead of equations (12) and (13)]. The true angular rate history was assumed perfectly measured by rate gyros and then integrated by 4-cycle Runge-Kutta. Instead of the Example 1 and 2 "attitude elements" $\{\phi_{co}(t_o), \theta_{co}(t_o), \psi_{co}(t_o); \omega_x(t_o), \omega_y(t_o), \omega_z(t_o)\}$, we successively improve instead the initial orientation angles $\{\phi_{co}(t_o), \theta_{co}(t_o), \psi_{co}(t_o)\}$ and the gyro bias parameters (b_x, b_y, b_z) . The numerical results were identical to Example 2, this test serves only to indicate the validity of the basic idea. This example was repeated, using perfect gyro data but imperfect image coordinates (with 1 mil measurement error variance). The converged pass points differed from their true values by an average of 1.8 ft. with a standard RMS error of 28.9 ft.

In real applications the effects of gyro bias and noise must also be considered. Thus, the final example of section 4.0 uses simulated gyro data (including bias and noise) a sequential (Kalman filter) estimation algorithm.

4.0 EXAMPLE 4 SEQUENTIAL TRIANGULATION SUBJECT TO DYNAMICAL CONSTRAINTS.

Based upon the formulation of section 2.5.2, a Kalman sequential triangulation algorithm has been developed. The 10 photo strip of examples 2 and 3 is selected as a basis for discussion and comparison of results. This particular computer program involves a significant amount of book-keeping to dynamically restructure the various matrices to correctly reflect the set of pass point coordinates being estimated on each cycle. As of this writing, this algorithm is still under development and test; it is anticipated that this work will culminate with successful numerical demonstrations in a few months. Although this particular portion of the work was in addition to the central objectives of this research project, the authors feel carrying it to completion will be a valuable contribution. This work will thus be discussed in a subsequent report, upon completion of the computational aspects.

5.0 CONCLUSIONS AND RECOMMENDATIONS

This report details several approaches to the dynamically constrained triangulation problem. The formulations are applied to obtain numerical results for several cases. These results support the following conclusions:

- (1) The most attractive method studied for batch triangulation is the direct rate integration approaches, as discussed in sections 2.2 and 3.3.
- (2) The sequential (extended Kalman filter) approach, discussed in sections 2.5 and 4.0, appears more attractive if
 - (a) *process noise* (due to, for example, integration of noisy gyro measurements) are degrading the solution to a considerable degree, and/or
 - (b) extremely long strips of photography are being triangulated.

We recommend that future refinement development of triangulation software include dynamical constraints in one of the two above fashions.

6.0 REFERENCES

1. Thompson, M. M., 1968 Manual of Photogrammetry, American Society of Photogrammetry, 3rd Ed., Vol. 1, p. 469.
2. Brown, D., 1968, "A Unified Lunar Control Network", Photogrammetric Engineering, 34: 12, pp. 1272-1292.
3. Brown, D., 1970, "The Rigorous and Simultaneous Adjustment of Lunar Orbital Photography", Rome Air Development Center Report RADC-TR-70-274.
4. Light, D. L., 1972, "Photo Geodesy from Apollo", Photogrammetric Engineering, 38: 6, pp. 547-587.
5. Hartwell, J. G., et al., 1973, "A Photogrammetric and Tracking Network Analysis Program", (FOTONAP), U.S. Army Engineers Topographic Laboratories Report ETL-CR-73-17.
6. Likins, P., Elements of Engineering Mechanics, McGraw-Hill, 1973, p. 105.
7. Blanton, J., and J. L. Junkins, 1976, "Dynamical Constraints in Satellite Photogrammetry", AIAA Preprint #76-824, presented to the AIAA/AAS Astrodynamics Conf., August, 1976, San Diego, CA.
8. Blanton, J. and J. L. Junkins, 1977, "Dynamical Constraints in Satellite Photogrammetry", AIAA Journal, Vol. 15, No. 4, pp. 488-499.
9. Blanton, J., and J. L. Junkins, 1977, "ERATTA: Dynamical Constraints in Satellite Photogrammetry", AIAA Journal, Vol. 15, No. 11, pp. 1663-1664.
10. Junkins, John L., 1978, Ch. 5 of Optimal Estimation of Dynamical Systems, Sithoff and Noordhoff Publishers, The Netherlands.

APPENDIX A

COORDINATE FRAME NOMENCLATURE AND KINEMATICAL RELATIONSHIPS

Important to any complex angular motion problem is the choice of orientation parameters and a clear, systematic nomenclature convention. The choice of orientation parameters is critical in that numerical difficulties may be avoided entirely or at least relegated to attitudes which will never occur in the problem at hand; a self-evident nomenclature is useful (particularly when several coordinate systems are defined) not only to readers but to the investigators themselves.

Throughout this research effort, Euler angles have been utilized for coordinate frame orientation. It is a well-known fact that each of the twelve possible Euler angle sets possesses a kinematical singularity. In order to render the singularity problem as harmless as possible, the Euler angle sequence for a given coordinate frame relative orientation has been selected so that encountering the singular orientation is highly unlikely. Future efforts could profitably involve the use of a four parameter orientation description (such as Euler parameters) so as to avoid the singularity problem entirely.

Unless there are reasons to the contrary, the 1-2-3 Euler angle sequence will be employed for simplicity of discussion. For future reference, the 3 x 3 transformation matrix [DE] orienting a frame D characterized by the orthonormal vector set

$$\{\underline{d}\} = \begin{Bmatrix} \underline{d}_1 \\ \underline{d}_2 \\ \underline{d}_3 \end{Bmatrix} \quad (A.1)$$

relative to a frame E characterized by

$$\{\underline{e}\} = \begin{pmatrix} \underline{e}_1 \\ \underline{e}_2 \\ \underline{e}_3 \end{pmatrix} \quad (\text{A.2})$$

has the form

$$[DE(\phi_{de}, \theta_{de}, \psi_{de})] = \begin{bmatrix} c\psi_{de} & s\psi_{de} & 0 \\ -s\psi_{de} & c\psi_{de} & 0 \\ 0 & 0 & 1 \end{bmatrix} \begin{bmatrix} c\theta_{de} & 0 & -s\phi_{de} \\ 0 & 1 & 0 \\ s\phi_{de} & 0 & c\phi_{de} \end{bmatrix} \begin{bmatrix} 1 & 0 & 0 \\ 0 & c\phi_{de} & s\phi_{de} \\ 0 & -s\phi_{de} & c\phi_{de} \end{bmatrix} \quad (\text{A.3})$$

where ϕ_{de} , θ_{de} , and ψ_{de} are the 1-2-3 Euler angles shown in Fig. 4 and

$c\theta_{de} = \cos\theta_{de}$, $s\theta_{de} = \sin\theta_{de}$, etc. The relationship between the two frames is compactly written as the matrix product

$$\{\underline{d}\} = [DE(\phi_{de}, \theta_{de}, \psi_{de})]\{\underline{e}\}. \quad (\text{A.4})$$

Obtainable from an elementary kinematic analysis of the frames displayed in Fig. A4 is the following matrix expression for the components (along the $\{\underline{d}\}$ unit vectors) of the angular velocity of frame D with respect to frame E:

$$\begin{pmatrix} \omega_1^{D/E} \\ \omega_2^{D/E} \\ \omega_3^{D/E} \end{pmatrix} = \begin{bmatrix} c\theta_{de}c\psi_{de} & s\psi_{de} & 0 \\ -c\theta_{de}s\psi_{de} & c\psi_{de} & 0 \\ s\theta_{de} & 0 & 1 \end{bmatrix} \begin{pmatrix} \dot{\phi}_{de} \\ \dot{\theta}_{de} \\ \dot{\psi}_{de} \end{pmatrix} \quad (\text{A.5})$$

Finally, both members of Eq. (A.5) may be premultiplied by the inverse of the 3 x 3 matrix on the right hand side to obtain expressions for the time rates of change of the Euler angles:

$$\begin{pmatrix} \dot{\phi}_{de} \\ \dot{\theta}_{de} \\ \dot{\psi}_{de} \end{pmatrix} = \frac{1}{c\theta_{de}} \begin{bmatrix} c\psi_{de} & -s\psi_{de} & 0 \\ c\theta_{de}s\psi_{de} & c\theta_{de}c\psi_{de} & 0 \\ s\theta_{de}c\psi_{de} & s\theta_{de}s\psi_{de} & c\theta_{de} \end{bmatrix} \begin{pmatrix} \omega_1^{D/E} \\ \omega_2^{D/E} \\ \omega_3^{D/E} \end{pmatrix} = [B(\theta_{de}, \psi_{de})] \begin{pmatrix} \omega_1^{D/E} \\ \omega_2^{D/E} \\ \omega_3^{D/E} \end{pmatrix} \quad (\text{A.6})$$

Contained in the above discussion are sub- and superscript conventions which, while appearing unnecessary in this simple context, will be utilized to great advantage in conjunction with the several coordinate frames about to be introduced.

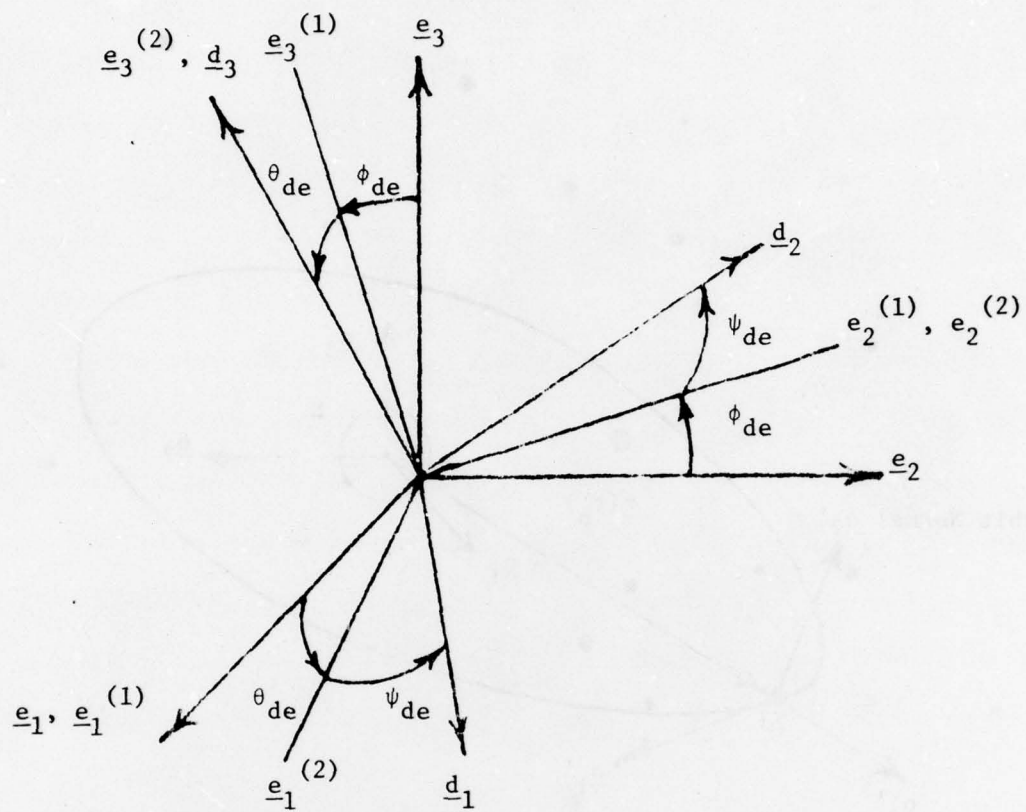


Fig. A1: A 1-2-3 Euler Angle Transformation

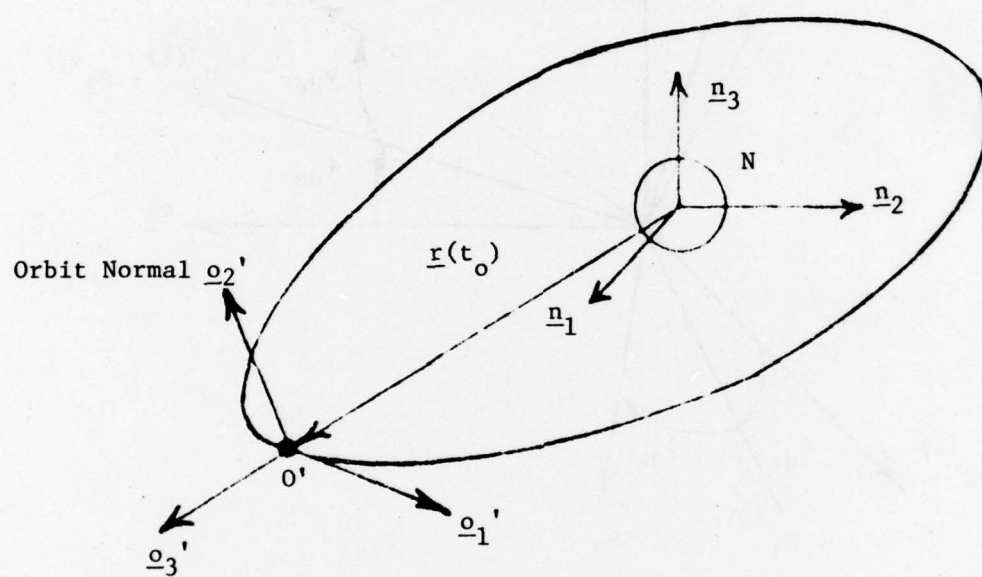


Fig. A2: The Inertial (N) and Orbit Inertial (O') Frames

We now turn to the first of the specific coordinate frames selected for use in the present problem. The inertial frame N (see Fig. A.2) is non-rotating and geocentric; it forms the basis for the on-board star catalog (if on-board star sensing capability exists) and is characterized by the unit vector set

$$\underline{n} = \begin{pmatrix} \underline{n}_1 \\ \underline{n}_2 \\ \underline{n}_3 \end{pmatrix} \quad (\text{A.7})$$

An "orbit inertial" frame O' (see Fig. A.2) is defined by the unit vectors

$$\begin{aligned} \underline{o}'_3 &= \frac{\underline{r}_o}{r_o} \\ \underline{o}'_2 &= \frac{\underline{r}_o \times \dot{\underline{r}}_o}{|\underline{r}_o \times \dot{\underline{r}}_o|} \end{aligned} \quad (\text{A.8})$$

$$\underline{o}'_1 = \underline{o}'_2 \times \underline{o}'_3,$$

where the subscript o denotes initial conditions. The $\{\underline{o}'\}$ unit vectors are projected onto the $\{\underline{n}\}$ unit vectors by the direction cosine matrix $[O'N]$ as

$$\{\underline{o}'\} = [O'N]\{\underline{n}\} \quad (\text{A.9})$$

The nine constant elements of $[O'N]$ are calculated from the orbit state vector by

$$\begin{aligned} O'N_{31} &= \frac{x_o}{r_o} \\ O'N_{32} &= \frac{y_o}{r_o} \\ O'N_{33} &= \frac{z_o}{r_o} \\ O'N_{21} &= \frac{h_1}{h} \\ O'N_{22} &= \frac{h_2}{h} \\ O'N_{23} &= \frac{h_3}{h} \end{aligned} \quad (\text{A.10})$$

$$0'N_{11} = 0'N_{22}0'N_{33} - 0'N_{23}0'N_{32}$$

$$0'N_{12} = 0'N_{23}0'N_{31} - 0'N_{21}0'N_{33}$$

$$0'N_{13} = 0'N_{21}0'N_{32} - 0'N_{22}0'N_{31},$$

$$\begin{aligned} \text{where } h_1 &= (y_o \dot{z}_o - z_o \dot{y}_o) \\ h_2 &= (z_o \dot{x}_o - x_o \dot{z}_o) \\ h_3 &= (x_o \dot{y}_o - y_o \dot{x}_o) \\ h &= (h_1^2 + h_2^2 + h_3^2)^{1/2} \end{aligned} \quad (A.11)$$

The orbit frame 0 (see Fig. A.3) rotates about \underline{o}_2' , the orbit normal, with the constant angular velocity (relative to N or 0')

$$\underline{\omega}^{0/N} = \underline{\omega}^{0/0'} = \Omega \underline{o}_2' = \Omega \underline{o}_2, \quad (A.12)$$

where Ω is given by

$$\Omega = \frac{2\pi}{(\text{orbit period})} = \frac{2\pi}{\sqrt{GM}} a^{3/2}. \quad (A.13)$$

GM is the earth gravitational-mass constant and a is the semi-major axis of the orbit. The $\{\underline{o}\}$ unit vectors are written in terms of the $\{0'\}$ unit vectors by

$$\{\underline{o}\} = [00'(t)]\{0'\}, \quad (A.14)$$

where

$$[00'(t)] = \begin{bmatrix} \cos[\Omega(t - t_o)] & 0 & -\sin[\Omega(t - t_o)] \\ 0 & 1 & 0 \\ \sin[\Omega(t - t_o)] & 0 & \cos[\Omega(t - t_o)] \end{bmatrix} \quad (A.15)$$

Substitution of Eq. (2.9) into Eq. (2.14) yields

$$\{\underline{o}\} = [00'(t)][0'N]\{\underline{n}\} \quad (A.16)$$

The next coordinate frame (G) considered is one attached to the strapped-down gyroscopic assembly and hence body-fixed but not necessarily principal. The G frame is generally considered to be the primary spacecraft axes. The unit vector set $\{\underline{g}\}$ of Fig. A.3 is characterized by \underline{g}_1 being the roll axis (nominally along the velocity vector),

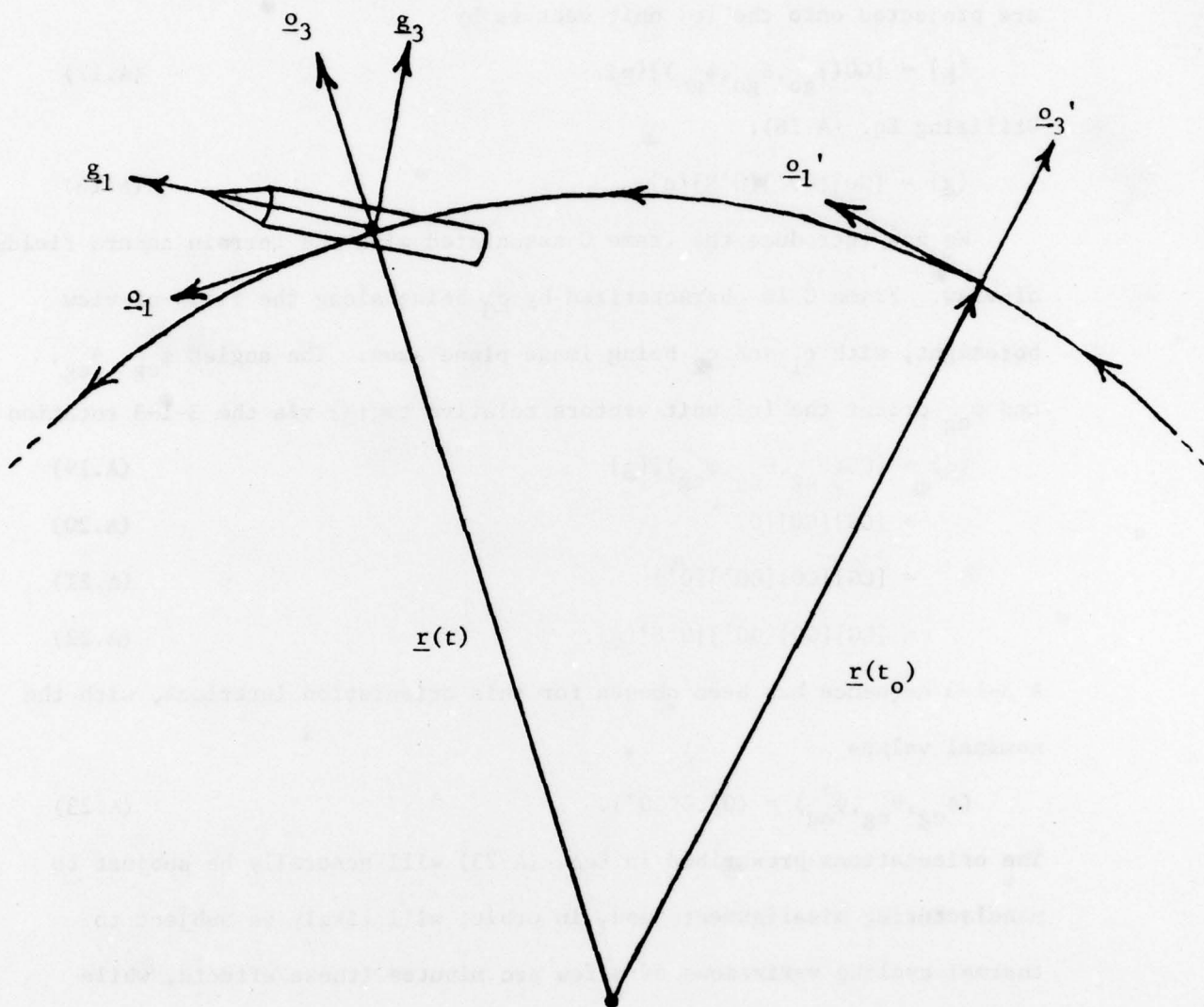


Fig. A3: The Orbit Frame O and Gyroscopic Frame G

\underline{g}_2 being the pitch axis (nominally along the orbit normal), and \underline{g}_3 being the yaw axis (nominally along the radius vector). The 1-2-3 angles ϕ_{go} , θ_{go} , and ψ_{go} orienting G relative to O are hence normally small, thereby avoiding the kinematical singularity at $\theta_{go} = 90^\circ$. The $\{\underline{g}\}$ unit vectors are projected onto the $\{\underline{o}\}$ unit vectors by

$$\{\underline{g}\} = [GO(\phi_{go}, \theta_{go}, \psi_{go})]\{\underline{o}\}. \quad (A.17)$$

Utilizing Eq. (A.16):

$$\{\underline{g}\} = [GO][00'] [0'N] \{\underline{n}\}. \quad (A.18)$$

We now introduce the frame C associated with the terrain camera fields-of-view. Frame C is characterized by \underline{c}_3 being along the field-of-view boresight, with \underline{c}_1 and \underline{c}_2 being image plane axes. The angles ϕ_{cg} , θ_{cg} , and ψ_{cg} orient the $\{\underline{c}\}$ unit vectors relative to $\{\underline{g}\}$ via the 3-1-3 rotation

$$\{\underline{c}\} = [CG(\phi_{cg}, \theta_{cg}, \psi_{cg})]\{\underline{g}\} \quad (A.19)$$

$$= [CG][GO]\{\underline{o}\} \quad (A.20)$$

$$= [CG][GO][00']\{\underline{o}'\} \quad (A.21)$$

$$= [CG][GO][00'] [0'N] \{\underline{n}\}. \quad (A.22)$$

A 3-1-3 sequence has been chosen for this orientation interlock, with the nominal values

$$(\phi_{cg}, \theta_{cg}, \psi_{cg}) = (0^\circ, 0^\circ, 0^\circ). \quad (A.23)$$

The orientations prescribed in Eqs. (A.23) will generally be subject to manufacturing misalignments and, in orbit, will likely be subject to thermal cycling variations of a few arc minutes (these effects, while important in applications, are not treated here; we note that their effects can be absorbed into slightly aliased biases, which are sequentially updated).

Finally, we introduce an "orbit C frame", designated C', which is coincident with frame A at the initial time t_0 , but which thereafter rotates about the orbit normal $\underline{o}_2 = \underline{o}_2'$ with the constant angular velocity

$$\underline{\omega}^{C'/N} = \underline{\omega}^{C'/O'} = \underline{\omega}_{O_2'} = \underline{\omega}_{O_2}. \quad (\text{A.24})$$

Frame C' represents the nominal position of camera frame C and is oriented relative to frame O via

$$\{\underline{c}'\} = c'^O(\phi_{c'o}, \theta_{c'o}, \psi_{c'o})\{\underline{o}\}, \quad (\text{A.25})$$

Where the 1-2-3 Euler angles $\phi_{c'o}$, $\theta_{c'o}$, and $\psi_{c'o}$ are constants (nominally zero). The relationship between the frames C and C' is given by

$$\{\underline{c}\} = [CC'(\phi_{cc'}, \theta_{cc'}, \psi_{cc'})]\{\underline{c}'\}, \quad (\text{A.26})$$

wherein the three 1-2-3 angles $\phi_{cc'}$, $\theta_{cc'}$, and $\psi_{cc'}$ are normally small.

Table A1 summarizes the coordinate system definitions and relationships discussed thus far.

The interlock angles (ϕ_{cg} , θ_{cg} , ψ_{cg}) will vary about their nominal calibrated values due to thermal cycling or any other structural deformation. The maximum amplitude of such variations is believed to be a few arc-minutes. We have not yet structured the estimation algorithms to provide updates of the interlock angles (ϕ_{cg} , θ_{cg} , ψ_{cg}). It is believed that noise in typical rate data (around one arc-sec/sec) is too large to allow significant refinement of (ϕ_{cg} , θ_{cg} , ψ_{cg}). As is noted in Section 4, these interlock angles are correlated with the estimated rate bias parameters, a fact which also hampers accurate estimation, but also makes their recovery less important; small interlock angle errors can be very nearly accounted for by absorbing these errors into slightly aliased rate biases (which, in themselves, are not of crucial importance).

Useful for consideration in incorporating attitude dynamical constraints are the time rates of change of various Euler angle sets in terms of the inertial angular velocity components of frame G. Specifically, we will develop expressions for

Table A1 REFERENCE FRAME SUMMARY

Designation	Unit Vectors	Associated With	Comments	Most Common Projections
N	$\{\underline{n}\}$	Inertial Frame	e.g., 1950 inertial system, or inertial system based upon equator and equinox of any specific date.	
O'	$\{\underline{o}'\}$	"Orbit Inertial" Frame	Coincides with O at the initial time t_0	$\{\underline{o}'\} = [O'N]\{\underline{n}\}$
O	$\{\underline{o}\}$	Uniform rotation about orbit normal	Rotation Ω is about $\underline{o}_2 = \underline{o}'_2$, the orbit normal	$\{\underline{o}\} = [OO']\{\underline{o}'\}$ $= [OO'] [O'N]\{\underline{n}\}$ $= [ON]\{\underline{n}\}$
G	$\{\underline{g}\}$	Gyro-fixed axes	\underline{g}_1 : roll axis \underline{g}_2 : pitch axis \underline{g}_3 : yaw axis	$\{\underline{g}\} = [GO]\{\underline{o}\}$ $= [GO][OO'] [O'M]\{\underline{n}\}$ $= [GN]\{\underline{n}\}$
C	$\{\underline{c}\}$	image plane of camera	\underline{c}_3 : along boresight $\underline{c}_1, \underline{c}_2$: image plane axes	$\{\underline{c}\} = [CG]\{\underline{g}\}$ $= [CG][GO][OO'] [O'N]\{\underline{n}\}$ $= [CN]\{\underline{n}\}$
C'	$\{\underline{c}'\}$	Uniform rotation of initial C frame about orbit normal	Rotation Ω is about $\underline{o}_2 = \underline{o}'_2$, the orbit normal; $[C'O] = [CO(t_0)]$	$\{\underline{c}'\} = [C'O]\{\underline{o}\}$ $= [C'O][ON]\{\underline{n}\}$ $= [C'N]\{\underline{n}\}$
E	$\{\underline{e}\}$	Earth fixed axes	\underline{e} , normal to equatorial plane, \underline{e}_1 through prime meridian	$\{\underline{e}\} = [EN]\{\underline{n}\}$ $\{\underline{c}\} = [CE]\{\underline{e}\}$

- (1) $(\dot{\phi}_{gn}, \dot{\theta}_{gn}, \dot{\psi}_{gn})$
- (2) $(\dot{\phi}_{cn}, \dot{\theta}_{cn}, \dot{\psi}_{cn})$
- (3) $(\dot{\phi}_{go}, \dot{\theta}_{go}, \dot{\psi}_{go})$
- (4) $(\dot{\phi}_{cc}, \dot{\theta}_{cc}, \dot{\psi}_{cc})$.

The relationships for the time rates of change of the angles

ϕ_{gn} , θ_{gn} , and ψ_{gn} follow directly from the form of Eqs. (A.6):

$$\begin{pmatrix} \dot{\phi}_{gn} \\ \dot{\theta}_{gn} \\ \dot{\psi}_{gn} \end{pmatrix} = \frac{1}{c\theta_{gn}} \begin{bmatrix} c\psi_{gn} & -s\psi_{gn} & 0 \\ c\theta_{gn}s\psi_{gn} & c\theta_{gn}c\psi_{gn} & 0 \\ s\theta_{gn}c\psi_{gn} & s\theta_{gn}s\psi_{gn} & c\theta_{gn} \end{bmatrix} \begin{pmatrix} \omega_1^{G/N} \\ \omega_2^{G/N} \\ \omega_3^{G/N} \end{pmatrix} = [B(\theta_{gn}, \psi_{gn})] \begin{pmatrix} \omega_1^{G/N} \\ \omega_2^{G/N} \\ \omega_3^{G/N} \end{pmatrix}. \quad (A.27)$$

Note that θ_{gn} , for the case of a near circular orbit and one vehicle rotation about g_2 per orbit, will go to 90° twice per orbit, causing $\cos\theta_{gn}$ to vanish with a resulting singularity in Eqs. (A.27).

The relationships for the time rates of change of the angles ϕ_{cn} ,

θ_{cn} , and ψ_{cn} can also be obtained from Eq. (A.6):

$$\begin{pmatrix} \dot{\phi}_{cn} \\ \dot{\theta}_{cn} \\ \dot{\psi}_{cn} \end{pmatrix} = [B(\theta_{an}, \psi_{an})][CG(\phi_{ag}, \theta_{ag}, \psi_{ag})] \begin{pmatrix} \omega_1^{G/N} \\ \omega_2^{G/N} \\ \omega_3^{G/N} \end{pmatrix} \quad (A.28)$$

The factor of $[CG]$ on the right side of Eq. (A.28) is necessary to convert the $\omega_1^{G/N}$ from components along $\{g\}$ axes to components along $\{c\}$ axes. Due to the form of the matrix B (defined in Eq. (A.6) and repeated in Eq. (A.27), singularities would occur twice per orbit for a vehicle which rotates about g_2 once per orbit. Hence, although fairly simple in form, Eqs. (A.27) and (A.28) share similar difficulties.

We now proceed to develop equations analogous to (A.27) and (A.28) for the angles $(\phi_{go}, \theta_{go}, \psi_{go})$ (Case 3). The angular velocity of G relative to N may be written as

$$\underline{\omega}_{G/N} = \underline{\omega}_{G/O} + \underline{\omega}_{O/N} \quad (\text{A.29})$$

or

$$\omega_1^{G/N} \underline{g}_1 + \omega_2^{G/N} \underline{g}_2 + \omega_3^{G/N} \underline{g}_3 = \dot{\phi}_{go}^{(1)} \underline{o}_1 + \dot{\theta}_{go}^{(2)} \underline{o}_2 + \dot{\psi}_{go} + \Omega \underline{o}_2, \quad (\text{A.30})$$

where the parenthetical superscripts indicate intermediate frames in the 0 to G transformation. Expressing $\underline{o}_1^{(1)}$, $\underline{o}_2^{(2)}$, and \underline{o}_2 in terms of \underline{g}_1 , \underline{g}_2 , and \underline{g}_3 enables one to equate coefficients of like unit vectors, resulting in three scalar equations which have the matrix form

$$\begin{pmatrix} \dot{\phi}_{go} \\ \dot{\theta}_{go} \\ \dot{\psi}_{go} \end{pmatrix} = [B(\theta_{go}, \psi_{go})] \begin{pmatrix} \omega_1^{G/N} \\ \omega_2^{G/N} \\ \omega_3^{G/N} \end{pmatrix} - \Omega \begin{pmatrix} c\phi_{go} s\psi_{go} + s\phi_{go} s\theta_{go} c\psi_{go} \\ c\phi_{go} c\psi_{go} - s\phi_{go} s\theta_{go} s\psi_{go} \\ -s\phi_{go} c\theta_{go} \end{pmatrix} \quad (\text{A.31})$$

For the case of one vehicle rotation about \underline{g}_2 per near circular orbit, the angles ϕ_{go} , θ_{go} , and ψ_{go} remain small so that Eqs. (A.31) are non-singular and nearly linear (important in the implementation of estimation algorithms).

To develop the Case 4 equations for $\dot{\phi}_{cc'}$, $\dot{\theta}_{cc'}$, and $\dot{\psi}_{cc'}$, we begin with

$$\underline{\omega}_{G/N} = \underline{\omega}_{C/C'} + \underline{\omega}_{C'/N}. \quad (\text{A.32})$$

Proceeding in a manner analogous to that outlined for Case 3, we arrive at

$$\begin{pmatrix} \dot{\phi}_{cc'} \\ \dot{\theta}_{cc'} \\ \dot{\psi}_{cc'} \end{pmatrix} = [B(\theta_{cc'}, \psi_{cc'})] [CG(\phi_{cg}, \theta_{cg}, \psi_{cg})] \begin{pmatrix} \omega_3^{G/N} \\ \omega_2^{G/N} \\ \omega_3^{G/N} \end{pmatrix} - \Omega [C'O(\phi_{c'o}, \theta_{c'o}, \psi_{c'o})] \begin{pmatrix} c\phi_{co} s\psi_{co} + s\phi_{co} s\theta_{co} c\psi_{co} \\ c\phi_{co} c\psi_{co} - s\phi_{co} s\theta_{co} s\psi_{co} \\ -s\phi_{co} c\theta_{co} \end{pmatrix}. \quad (\text{A.33})$$

Like Eqs. (A.31), Eqs. (A.33) are more complex than Eqs. (A.27) or (A.28) but offer the advantages of near linearity and no singularities for the case of one vehicle rotation about g_2 per orbit.

Unclassified

SECURITY CLASSIFICATION OF THIS PAGE (When Data Entered)

REPORT DOCUMENTATION PAGE		READ INSTRUCTIONS BEFORE COMPLETING FORM
1. REPORT NUMBER	2. GOVT ACCESSION NO.	3. RECIPIENT'S CATALOG NUMBER
4. TITLE (and Subtitle) ORBITAL PHOTOGRAMMETRIC TRIANGULATION WITH DYNAMICAL CONSTRAINTS		5. TYPE OF REPORT & PERIOD COVERED
7. AUTHOR(s) John L. Junkins Mahesh Rajan James D. Turner		6. PERFORMING ORG. REPORT NUMBER
9. PERFORMING ORGANIZATION NAME AND ADDRESS Engineering Science and Mechanics Department Virginia Polytechnic Institute and State Univ. Blacksburg, VA 24061		8. CONTRACT OR GRANT NUMBER(s) DAAG29-77-0018 ✓ DAAG29-78-0043
11. CONTROLLING OFFICE NAME AND ADDRESS U. S. Army Research Office P. O. Box 12211 Research Triangle Park, NC 27709		10. PROGRAM ELEMENT, PROJECT, TASK AREA & WORK UNIT NUMBERS March 1979
14. MONITORING AGENCY NAME & ADDRESS (if different from Controlling Office)		12. REPORT DATE
		13. NUMBER OF PAGES
		15. SECURITY CLASS. (of this report) Unclassified
		15a. DECLASSIFICATION/DOWNGRADING SCHEDULE
16. DISTRIBUTION STATEMENT (of this Report) Approved for public release; distribution unlimited.		
17. DISTRIBUTION STATEMENT (of the abstract entered in Block 20, if different from Report)		
18. SUPPLEMENTARY NOTES The view, opinions, and/or findings contained in this report are those of the author(s) and should not be construed as an official Department of the Army position, policy, or decision, unless so designated by other documentation.		
19. KEY WORDS (Continue on reverse side if necessary and identify by block number) Triangulation, Estimation, Photogrammetry		
20. ABSTRACT (Continue on reverse side if necessary and identify by block number) The concept, implementation, and results of incorporating spacecraft motion constraints into the process of triangulating orbital photography is investigated. Feasibility and desirability several approaches to this problem are established relative to conventional unconstrained triangulation.		

79